1.0

1.1

1.25 1.4 1.6

45
50
56
63

2.8 2.5
3.2 2.2
36
40 2.0

1.8

MICROCOPY RESOLUTION TEST CHART
NATIONAL BUREAU OF STANDARDS-1963-A

LEVEL II

THE EFFECT OF PREDEFORMATION ON THE CREEP BEHAVIOR
AND RUPTURE LIFE OF MA 754

ROBERT THOMAS MARLIN

Submitted in partial fulfillment
of the requirement for
The Degree of Master of Science
in the School of Engineering and Applied Science
Columbia University

- 1979 -

80 10 16 092

REPORT DOCUMENTATION PAGE		READ INSTRUCTIONS BEFORE COMPLETING FORM
1. REPORT NUMBER 79-179T	2. GOVT ACCESSION NO. AD-A091 458	3. RECIPIENT'S CATALOG NUMBER (14) AFIT-CI-79-179T
4. TITLE (and Subtitle) The Effect of Predeformation on the Creep Behavior and Rupture Life of MA 754		5. TYPE OF REPORT & PERIOD COVERED Thesis
		6. PERFORMING ORG. REPORT NUMBER
7. AUTHOR(s) 2Lt Robert Thomas Marlin		8. CONTRACT OR GRANT NUMBER(s) Master's thesis,
9. PERFORMING ORGANIZATION NAME AND ADDRESS AFIT Student at: Colombia University NY		10. PROGRAM ELEMENT, PROJECT, TASK AREA & WORK UNIT NUMBERS
11. CONTROLLING OFFICE NAME AND ADDRESS AFIT/NR WPAFB OH 45433		12. REPORT DATE 1979
		13. NUMBER OF PAGES 34
14. MONITORING AGENCY NAME & ADDRESS(if different from Controlling Office)		15. SECURITY CLASS. (of this report) UNCLASS
		15a. DECLASSIFICATION/DOWNGRADING SCHEDULE

16. DISTRIBUTION STATEMENT (of this Report)

Approved for public release; distribution unlimited

17. DISTRIBUTION STATEMENT (of the abstract entered in Block 20, if different from Report)

APPROVED FOR PUBLIC RELEASE AFR 190-17.

FREDRIC C. LYNCH, Major, USAF
Director of Public Affairs

23 SEP 1980

18. SUPPLEMENTARY NOTES

Approved for public release; IAW AFR 190-17

Air Force Institute of Technology (ATC)
Wright-Patterson AFB, OH 45433

19. KEY WORDS (Continue on reverse side if necessary and identify by block number)

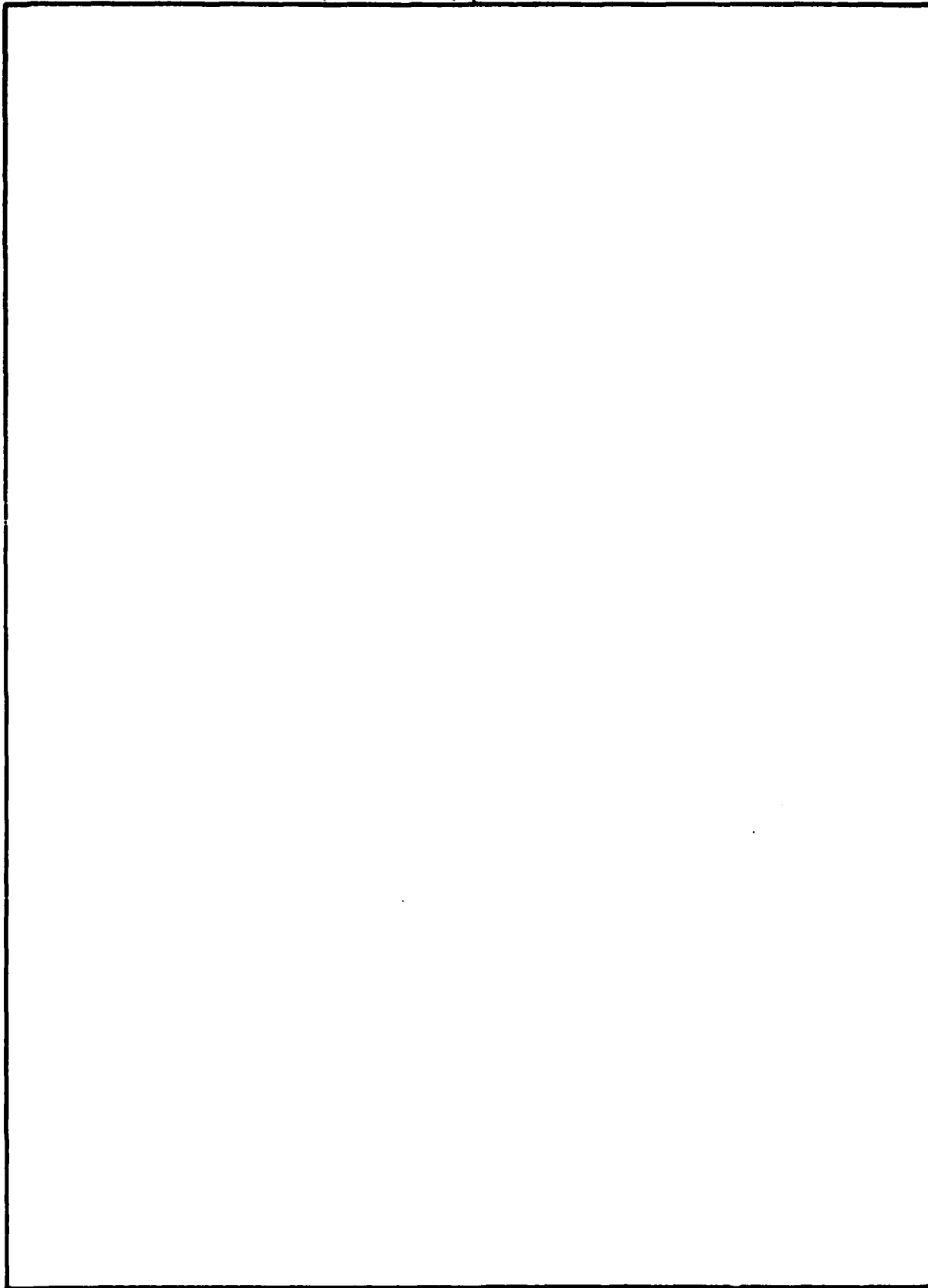20. ABSTRACT (Continue on reverse side if necessary and identify by block number)

Attached

DD FORM 1473 1 JAN 73   EDITION OF 1 NOV 65 IS OBSOLETE

TABLE OF CONTENTS

Accession For

NTIS GRA&I
DDC TAB
Unannounced
Justification

By

Distribution/

Availability Codes

Dist. | Avail and/or
        | special

A

ABSTRACT

THE EFFECT OF PREDEFORMATION ON THE CREEP
BEHAVIOR AND RUPTURE LIFE OF MA 754
ROBERT THOMAS MARLIN

Tests were conducted on a nickel-base superalloy after prede-
forming the material by applying a high strain (2×10^{-5} sec^{-1}) to
the specimens before creep testing. The effect of the predeforma-
tion on the creep behavior and stress rupture life was evaluated.

The material tested was a nickel-base, oxide dispersion strength-
ened solid solution alloy developed by the International Nickel Com-
pany and called MA 754.[*] The material is formed by mechanical alloy-
ing and powder metallurgy techniques.

After predeforming the specimens by applying a 276 MPa stress
until the desired amount of prestrain was attained, the specimens were
crept at 224 MPa until failure. Both predeformation and creep test-
ing were conducted at 760°C.

The minimum creep rate decreased as the amount of prestrain ap-
plied increased and was a factor of two lower than the standard at
1.2% prestrain. Also, the prestrained specimens reached their minimum
creep rates in a shorter period of time than the standard specimens.
The rupture life increased with increasing amounts of prestrain up to
0.6% prestrain and then decreased with further prestrain, but was still
slightly greater than the life of the standard at 1.2% prestrain.

Transmission electron microscopy revealed dislocations being emit-
ted from particle-matrix interfaces and an apparent increase in dislo-
cation density with increasing amounts of prestrain. The observations
suggest that a dispersion hardening effect may be occurring.

-ii-

*trademark

ACKNOWLEDGEMENTS

LIST OF FIGURES

LIST OF TABLES

I. INTRODUCTION

The influence of notches on the creep rupture strength of an oxide dispersion strengthened (ODS) alloy has been demonstrated.[1] The study used normal notched bars ($K_t = 3$) and sharp-edged notched sheet ($K_t = 10$) of an ODS alloy and found a notch strengthening effect in both cases. Two possible explanations for the strengthening are offered. 1) Smooth bar fracture occurs by grain boundary sliding and transverse grain boundary delamination. Due to a high grain aspect ratio of approximately 10 to 1, the region affected by the notch is small compared to the average longitudinal grain length and a smaller number of transverse grain boundaries may be affected. 2) The stress concentration at the notch tip may cause a change in the creep and stress rupture properties of the material surrounding the notch.

A study has been done to determine the stress redistribution in notched bars during creep testing.[2] The study showed that the strain rate is initially very high in the region near the notch tip and decreases as the distance from the tip increases. After a period of time a stationary state exists and the strain rate is fairly uniform throughout the section due to stress relief during creeping. By predeforming specimens using a high stress and then reducing the stress and creep testing, the conditions at the notch tip can be simulated.

In order to determine if the creep and rupture properties are affected by the high stresses around a notch tip, predeformation tests were done on the ODS alloy MA 754.

II. EXPERIMENTAL PROCEDURE

A. Material

INCONEL alloy* MA 754 was used for all tests. MA 754 is a nickel-base solid solution alloy strengthened by a small volume fraction of yttrium oxide dispersoids. Table 1 lists the nominal chemical composition of the alloy. After mechanical alloying and consolidation of the powder by extrusion, the material receives a moving zone heat treatment in order to develop elongated grains.[3] It is then rolled into a 2.8 x 8.3 cm billet and given a standard high temperature heat treatment of 1316°C / 2 hrs / air cool which coarsens the grain structure.

Specimens were machined from heat treated bar stock material and were cut parallel to the extrusion axis. All specimens had a nominal gage length of 12.70 mm and a nominal gage diameter of 3.18 mm. The gage diameter of each specimen was determined to within ±0.01 mm with a micrometer, and the load set on the creep machine was based on this measurement. Specimens were photographed and enlarged, and the actual gage length, defined as the section of constant diameter bounded by radiused fillets, was calculated to within ± 0.1 mm.

Samples of virgin material and post-crept specimens were polished on progressively finer papers to 1 μm diamond grit, then electrolytically or chemically etched. Optical microscopy was done on a Zeiss Ultraphot II microscope.

For transmission electron microscopy, thin slices approximately 0.35 mm thick were cut using a diamond saw, mechanically ground down to 0.05 mm and electrothinned until perforation occurred using a Fishione Model 120 automatic jet polisher. The foils were examined in a JEOLCO transmission electron microscope (Model JEM-100C) operating at

* Trademark of the International Nickel Company

Table 1. Nominal chemical composition of MA 754

Ni	Cr	Fe	Ti	Al	C	Y_2O_3	O
76.8	20.1	1.4	0.5	0.25	0.06	0.6	0.3

100 Kv.

The grain structure of MA 754 is shown in figure 1. The grains
have long and short transverse grain sizes of about 60 and 45 μm re-
spectively, and a grain aspect ratio of approximately 10 to 1.

Figure 2 shows the microstructure of the as-received material.
The microstructure of MA 754 consists of a dispersion of yttrium oxides,
twins, and coarser inclusions thought to be carbides or carbonitride
phases.[4-5] The coarser inclusions occur randomly throughout the matrix
and at grain boundaries.

B. Equipment and Creep Testing Procedure

All creep tests were done using an Amsler type STFM 746 lever
arm testing machine with manual realignment capability. Universal
joints (two degrees of rotational freedom) were used in the load train
to further minimize bending moments. The machine was periodically cal-
ibrated with a 500 lb. load cell to insure that the applied load re-
sulted in the proper stress. The temperature was continuously moni-
tored using a strip chart recorder with an electronic cold junction
corrected chromel-alumel thermocouple. The furnace temperature at the
specimen was controlled to within ± 3.0°C. The typical temperature
gradient along the short gage length is less than 1°C.

Creep strains were monitored with a Hewlett-Packard linear var-
iable displacement transducer (LVDT) linked to an Omniscribe strip
chart recorder. An internal extensometer measured the strain to with-
in 0.001 percent.

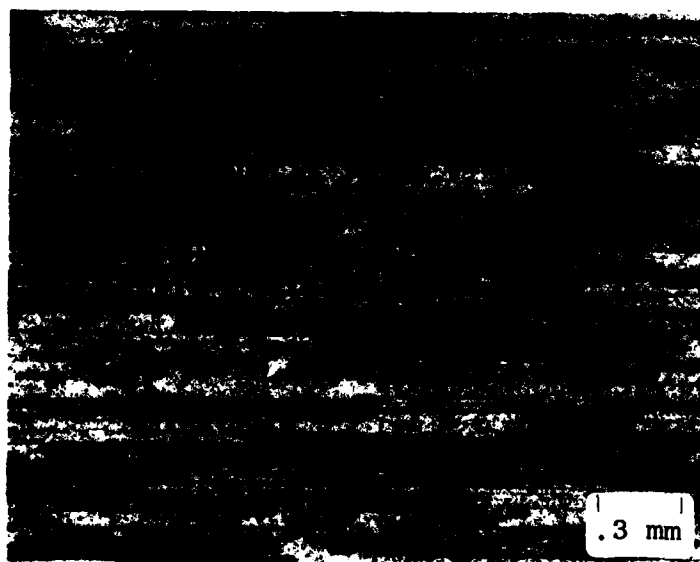The specimens were predeformed by applying a stress of 276 MPa

a

b

Fig. 1. Photomicrographs of the grain structure of
MA 754 showing the a) long transverse and longitudinal
grain dimensions, and b) the short transverse and long-
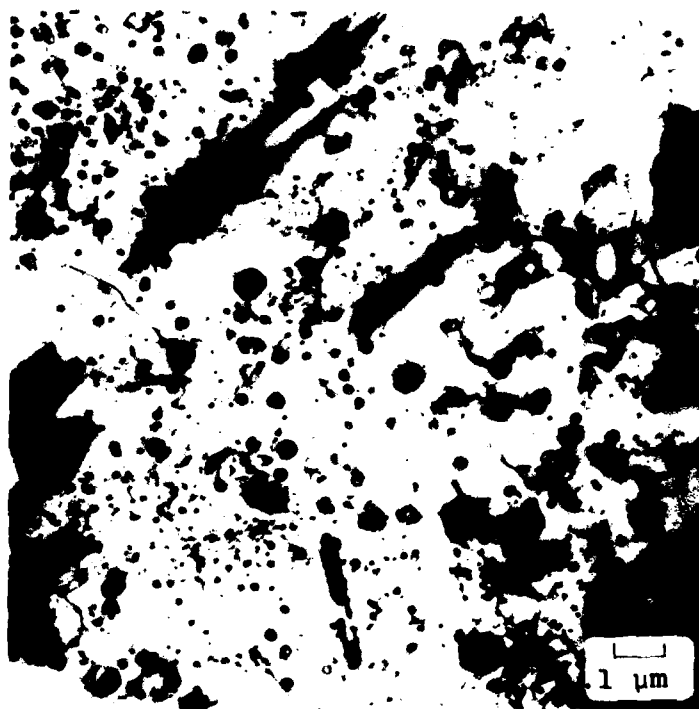itudinal grain dimensions.

Fig. 2. Transmission electron micrograph of as-received MA 754 showing the oxide dispersion.

at 760°C until a desired amount of strain was attained. Prestrain values of 0.3%, 0.6%, 0.9%, and 1.2% were chosen. The load was then carefully removed and reduced to give a stress of 224 MPa. The specimens were then crept to failure at 760°C.

For each test a steady state creep rate was determined with a computer program that fitted a straight line to the strain and time measurements taken between the inflection points marking the end of primary and the beginning of tertiary creep and found the slope of this line. The technique used was linear regression by the method of least squares.

C. Error

Systematic errors in the strain and strain rate measurements can arise from errors in LVDT calibration and from the output of the strip chart recorder. Random errors may stem from gage length measurement on specimen photographs, micrometer measurement of the gage diameter, and estimation of fractions of divisions on the strip chart. By taking the square root of the sum of the squares of all the errors defined above[6], the accuracy of any strain rate is found to be at most ± 5.0 percent of the strain rate.

Errors in applied stress can result from errors in weight placement on the lever arm and errors in gage diameter measurement. The applied stresses are accurate to within ± 1.4 percent of the stress magnitude in the worst case.

Errors in the amount of prestrain applied can arise from difficulty in determining the exact elastic to plastic deformation point and from estimation of fractions of divisions on the strip chart.

III. EXPERIMENTAL RESULTS

A typical creep curve for the creep conditions of 276 MPa and 760°C is presented in figure 3 and shows that the amounts of prestrain all fall within the primary creep region of the curve. Consequently, there should be no cracking in the specimens during the predeformation process. Examination of specimens after prestraining revealed no obvious grain structure changes or cracking of grain boundaries.

A plot of minimum creep rate at 224 MPa versus amount of prestrain at 276 MPa shows that the minimum creep rate decreases with increasing amounts of prestrain and is lower than the standard specimen minimum creep rate by a factor of two at 1.2% prestrain (Figure 4).

Figure 5 shows that the average stress rupture life at 224 MPa increases with increasing amounts of prestrain until 0.6% prestrain. After 0.6% prestrain the rupture life decreases, but is still slightly greater for the 1.2% prestrained specimens than the rupture life of the standard specimens.

A set of higher minimum creep rate values exist as shown by the dashed line in figure 4. The higher creep rates also decrease with increasing amounts of prestrain.

As shown in figure 5, the rupture lives corresponding to the higher creep rates (dashed curve) increase from a value lower than the average standard specimen rupture life at 0.3% prestrain.

A plot of strain rate versus time shows that the time to reach the minimum creep rate decreases as the amount of prestrain increases (Figure 6). The minimum creep rate for the 0.6% prestrained test is lower than the standard minimum creep rate, and the rupture life is substantially increased. The 1.2% prestrained test minimum creep
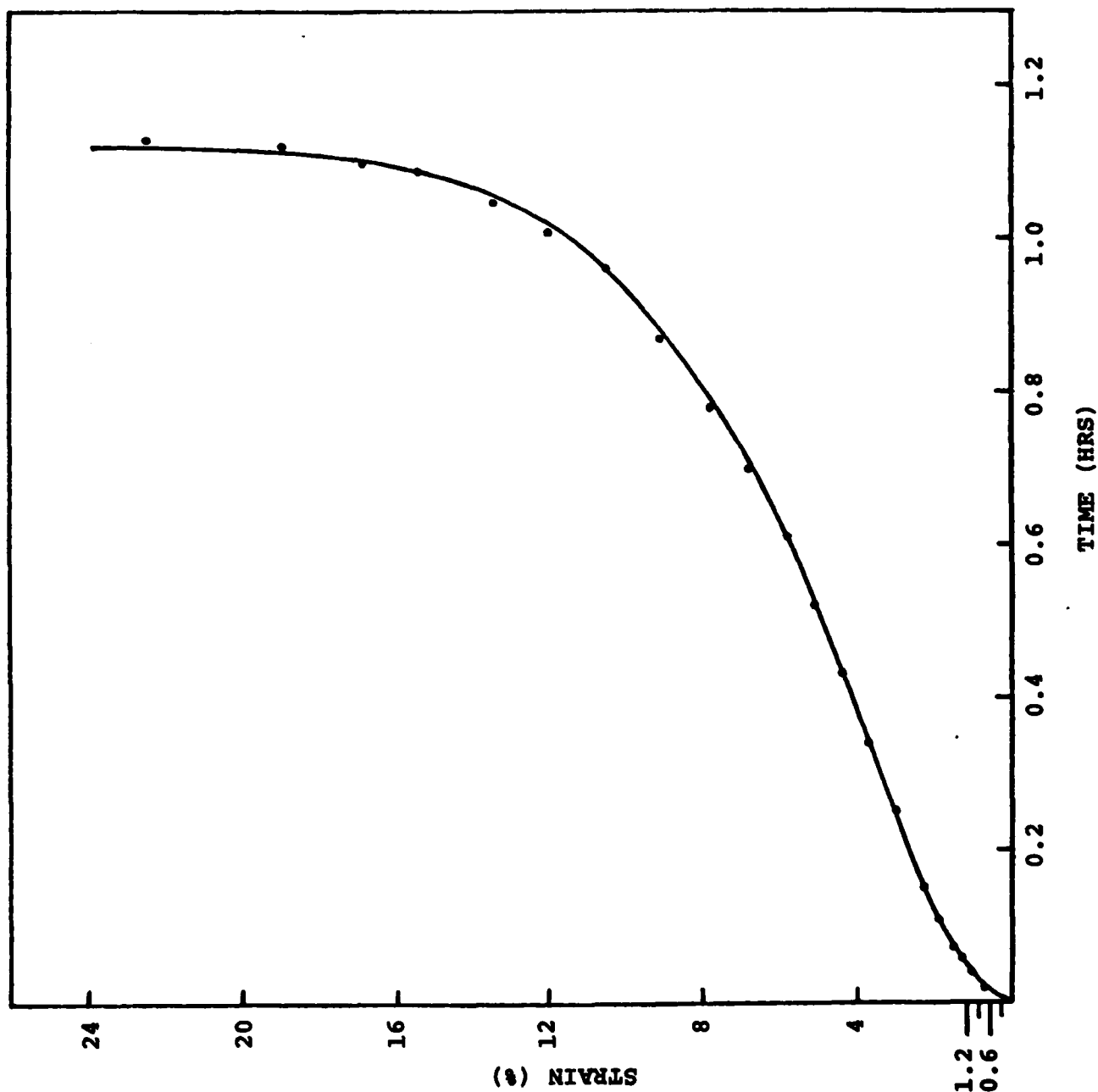
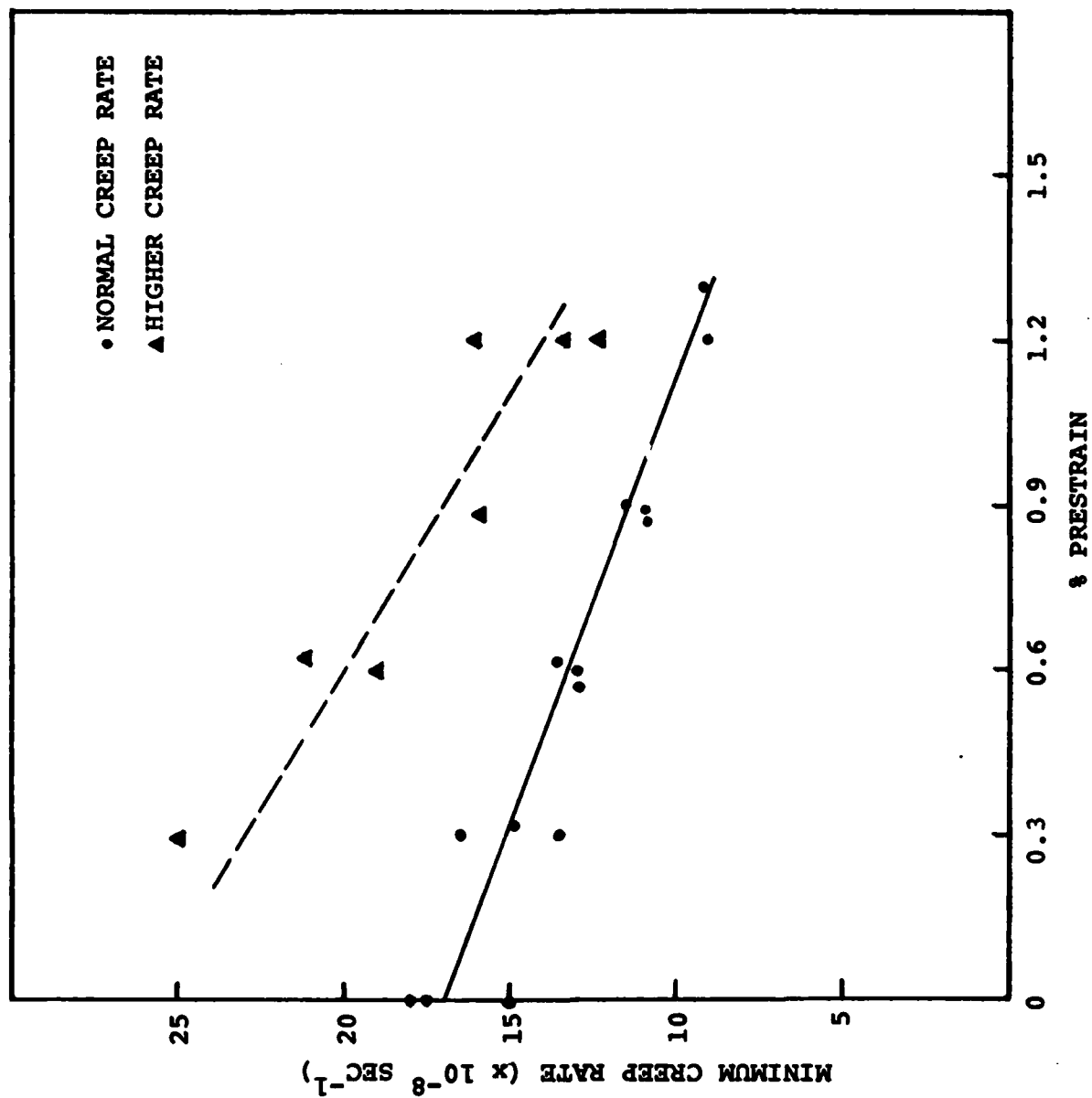Fig. 3. Typical creep curve for the creep conditions of 276 MPa and 760°C.

Fig. 4. Graph of minimum creep rate at 224 MPa versus amount of prestrain at 276 MPA.
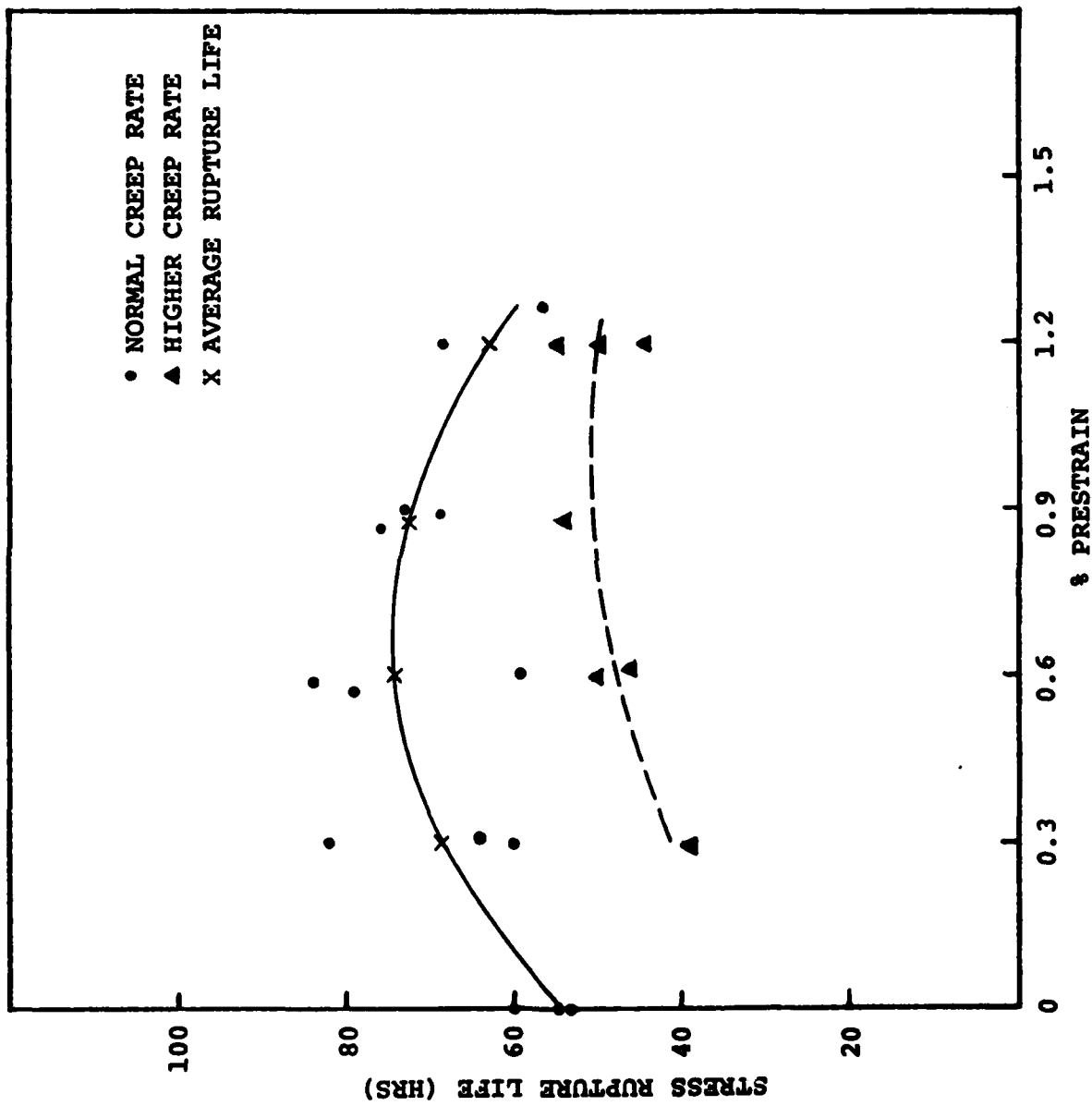
Fig. 5. Graph of stress rupture life at 224 MPa versus amount of prestrain at 276 MPa.
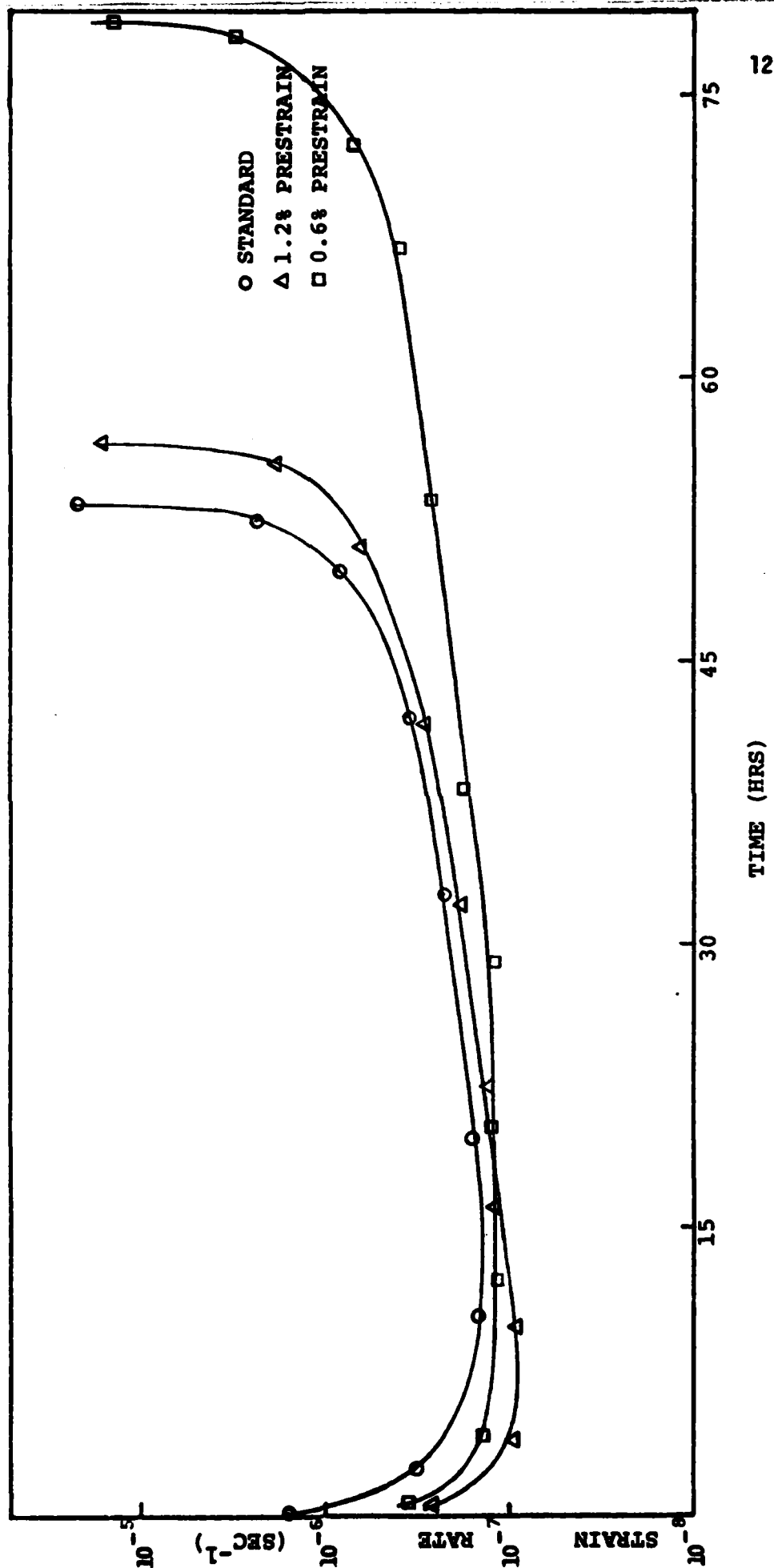
Fig. 6. Strain rate versus time plot of standard, 0.6%,
and 1.2% prestrained specimens.

12

rate is lower than the 0.6% test, but the creep rate increases after a short period of time, and the strain rate versus time curve roughly parallels the standard specimen curve. The rupture life of the 1.2% test is slightly greater than that of the standard.

Figure 6 also shows that in the late tertiary stage of creep the creep rate accelerates leading to failure in all tests. A table of the time until a creep rate of 1×10^{-6} per second occurs and the corresponding total strain at that point reveals that the creep rate accelerates when a total accumulated strain of 6.6% is reached (Table 2). The value is independent of the creep rates or the rupture lives of the specimens. Table 3 is a similar display of the time until the beginning of the tertiary stage of creep and the total accumulated strain at that point. The tertiary stage also begins at a constant accumulated strain value, independent of creep rate and rupture life.

Failure of the specimens occurs by crack formation and delamination at transverse grain boundaries. Figure 7 is a photomicrograph showing transverse grain boundary cracking in a specimen crept to failure at 224 MPa.

Figure 8 is a transmission electron microscopy (TEM) micrograph of a specimen showing dislocations being emitted from a carbide-matrix interface.

From TEM micrographs of the standard, 0.6%, and 1.2% prestrained specimens, the approximate dislocation density was calculated using a method documented by Hirsch et al.[6] Due to variations in foil thickness and the variation in dislocation density around twins and particles, the calculated dislocation densities are approximate. However, the density values can still be used for relative comparisons. Figure 9 is a graph of the average dislocation density versus the amount of

Table 2. Time until accelerated creep rate and
corresponding strain.

CONDITION	TIME UNTIL $\dot{\varepsilon} = 1 \times 10^6 \text{ s}^{-1}$ (HRS)	%ε AT 224 MPa	TOTAL %ε (IN- CLUDING PRE ε)
STD	53	6.3	6.3
0.3%	62	6.4	6.7
0.6%	81	6.5	7.1
0.9%	70	5.8	6.7
1.2%	66	5.2	6.4
			6.6 AVG

Table 3. Time until tertiary creep and corresponding strain.

CONDITION	TIME UNTIL TERTIARY CREEP (HRS)	$\%\epsilon$ AT 224 MPa	TOTAL $\%\epsilon$ (INCLUDING PRE ϵ)
STD	18	1.8	1.8
0.3%	25	1.7	2.0
0.6%	27	1.4	2.0
0.9%	26	1.2	2.1
1.2%	15	0.8	2.0
			2.0 AVG

Fig. 7. Photomicrograph showing transverse grain boundary cracking in a specimen crept to failure at 224 MPa.
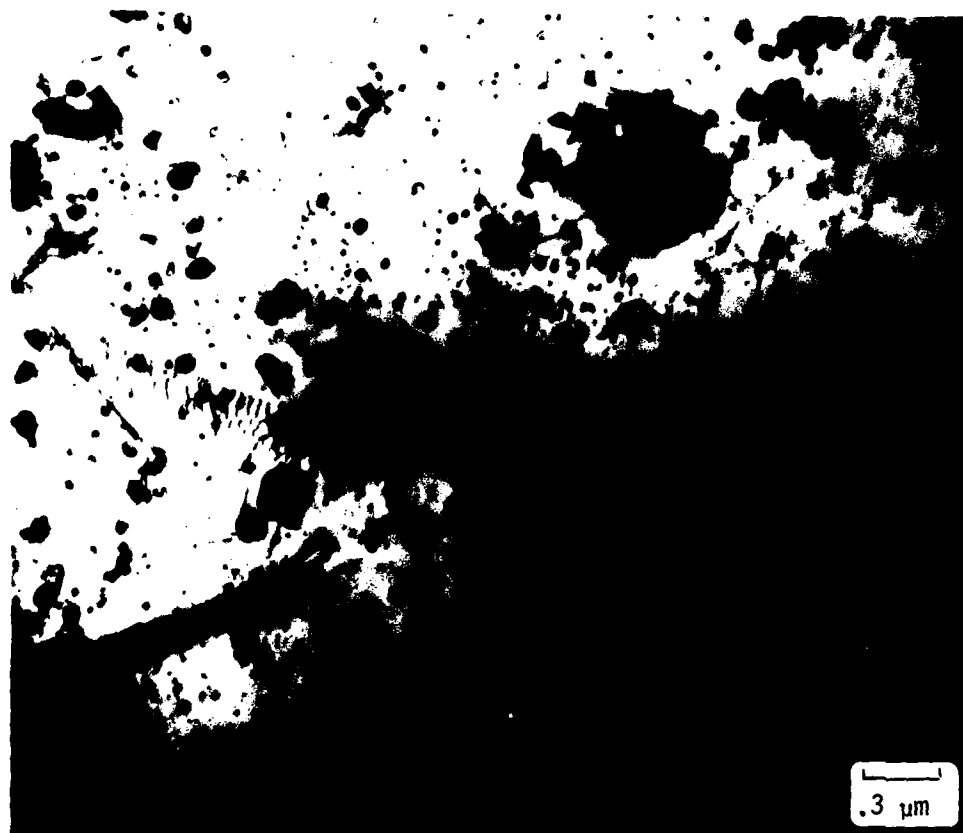
Fig. 8. TEM micrograph of dislocations being emitted from a carbide-matrix interface.

prestrain and shows that the dislocation density increases with increasing amounts of prestrain.

Figure 10 is a TEM micrograph of the area just below the fracture surface of a specimen crept to failure at 224 MPa and shows a high dislocation density and the absence of any dislocation substructure.
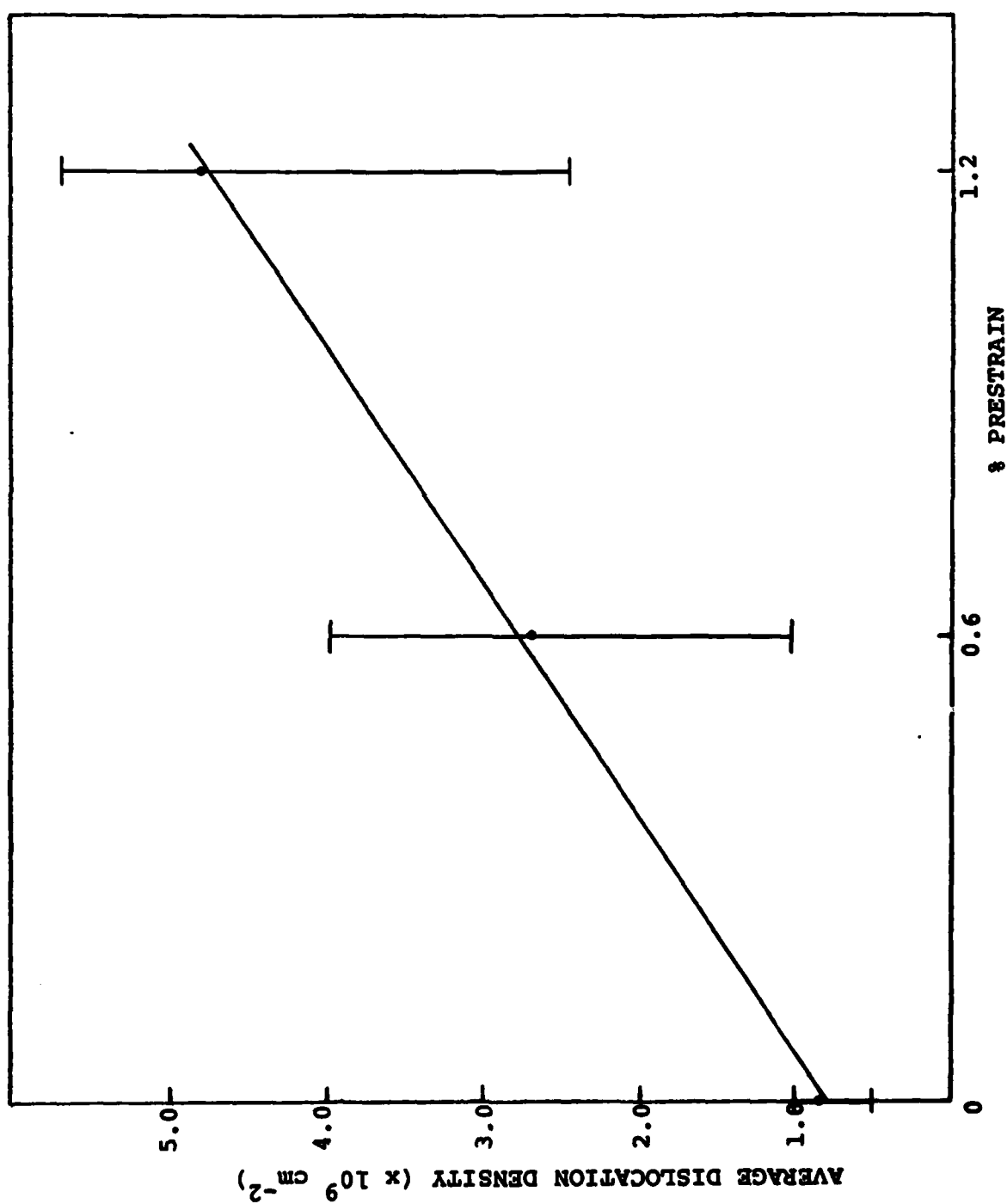
Fig. 9. Plot of average dislocation density versus amount of prestrain.

Fig. 10. TEM micrograph of the area below the fracture surface of a specimen crept to failure at 224 MPa.

IV. DISCUSSION

The decrease in minimum creep rate can be attributed to a dispersion hardening effect. Local shear stresses develop around MC carbides (Cr, Ti) during the predeformation phase of the test, and in order to accommodate the stresses, localized slip occurs in the region of the carbides and dislocations are emitted from the particle-matrix interface. In this way the carbides become dislocation sources. The process by which dislocations are emitted from the particle and metal matrix interface has been reported by Ashby, Gelles, and Tanner.[8] The increase in dislocation density with increasing amounts of pre-strain and the high dislocation density at failure suggest that the dislocation sources operate during the entire course of the test.

The carbides generate dislocations which are pinned by the incoherent yttrium oxide dispersoids and thereby increase the creep resistance of the material. As the amount of prestrain increases, more dislocations are generated and immobilized and, hence, the lower minimum creep rate.

As previously shown in tables 2 and 3, the tertiary stage of creep begins at approximately 2% total accumulated strain, and the accelerated tertiary stage begins at roughly 6.6% total strain. Pre-vious studies on MA 754 have shown an apparent strain controlled failure criterion,[9] and this investigation supports the findings.

The time to attain the minimum creep rate decreases as the amount of prestrain increases due to the greater amount of strain accumulated in a shorter period of time during the high strain rate (2×10^{-5} sec^{-1}) process of prestraining. In other words, after the prestrain, less accumulated strain is needed in order to reach the total strain value

that identifies the end of the primary stage of creep, and less time is needed to reach that value of strain under the 224 MPa creep condition.

As previously mentioned and shown in figure 6, the minimum creep rate for the 1.2% prestrained test is a factor of two lower than that of the standard specimen, but the rupture life is only slightly greater than that of the standard. On the other hand, the minimum creep rate for the 0.6% prestrained specimen is only slightly less than that of the standard, but the rupture life is significantly longer. At 1.2% prestrain, the accumulated strain reaches the value needed for cracking and delamination of the transverse grain boundaries (tertiary stage of creep) after a short period of time. Transverse grain boundary cracking and delamination occur and the creep rate increases causing a rupture life only slightly greater than that of the standard specimen. The 0.6% prestrained sample has a higher minimum creep rate than the 1.2%, but perhaps more importantly, the total accumulated strain is less. The creep resistance of the material is increased and more time is needed to reach the total strain necessary for the beginning of the tertiary stage of creep. Consequently, the rupture life is significantly extended.

The scatter in the rupture lives of the specimens (Figure 5) can be attributed to specimen to specimen differences in crack initiation and crack propagation rate along transverse grain boundaries.

The higher creep rates observed at the prestrained conditions (dashed line in figure 4) may be caused by a higher defect density in some of the specimens. A test with a creep rate that was over twice the average minimum creep rate of the specimens at the same prestrain condition was interrupted after 11.5 hours and showed a number of large inclusions in the matrix (Figure 11). The grain size
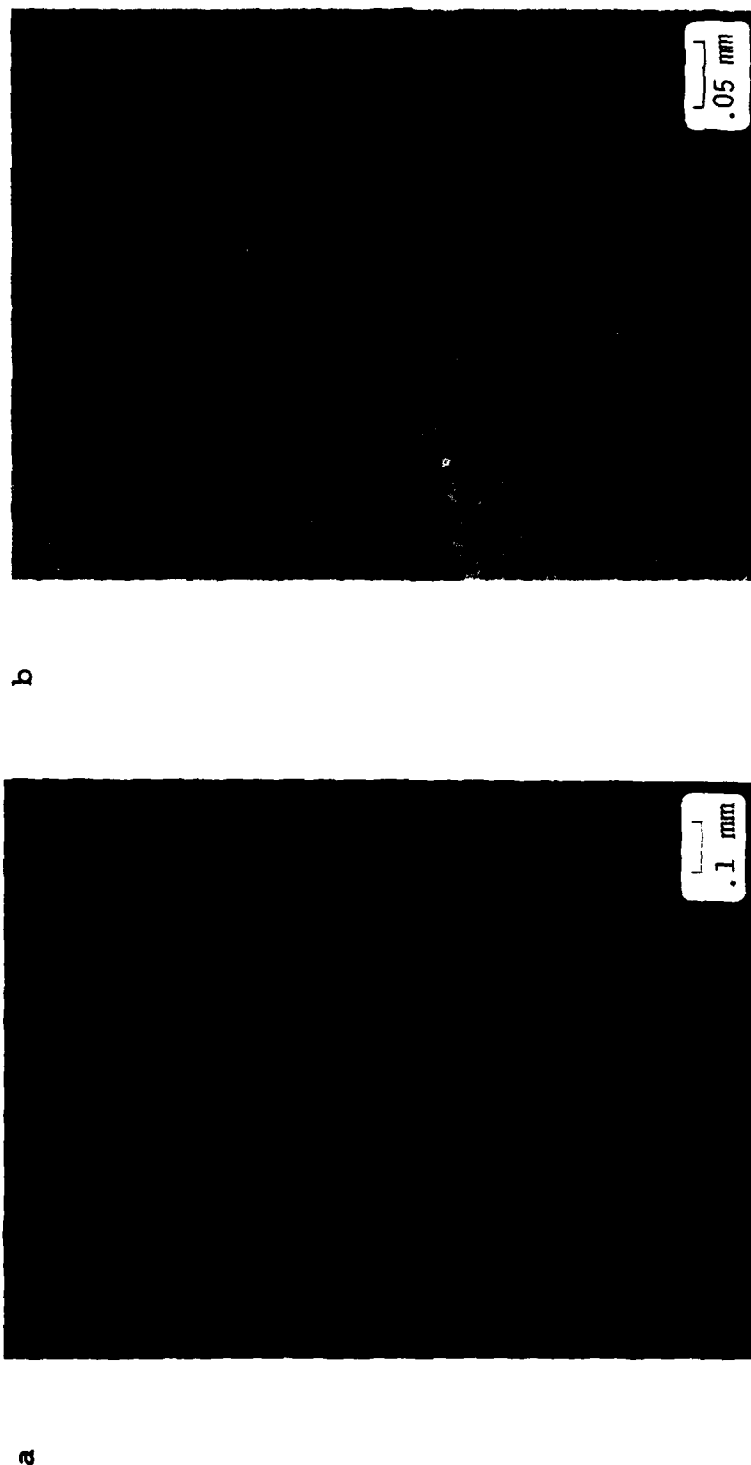
b

.05 mm

a

.1 mm

Fig. 11. Photomicrographs of a specimen from a test interrupted at 11.5 hrs showing large inclusions in the matrix.

is considerably smaller around the inclusions, and transverse grain boundary cracking is observed in the vicinity of the inclusions. The inclusions are found in the as-received material as well as the crept specimens and may be produced during the extrusion phase of the fabrication process.

A high density of smaller inclusions may weaken the material and decrease the creep resistance in a similar manner to that of the larger inclusions but with less drastic consequences. Figures 12-15 are optical photomicrographs of specimens crept to failure after being prestrained to 0.6%, cut longitudinally, and polished. Figures 12 and 13 are from a specimen with a minimum creep rate comparable to the average minimum creep rate at that condition. The highest density of transverse grain boundary cracks occurs near the fracture surface and decreases as the distance from the fracture surface increases. Figures 14 and 15 are from a specimen with a minimum creep rate of nearly twice the average creep rate. Figure 14 reveals a large inclusion in the matrix, but of more significance is the transverse grain boundary cracking away from the fracture surface and a considerably lower crack density near the fracture surface. Figure 15 also shows a large number of cracks in the matrix. A high defect density may be weakening the material and contributing to the formation of cracks away from the fracture surface. A number of longitudinal inclusions are visible in all the photomicrographs, but a judgment on the density of the small inclusions cannot be made.

The defects may decrease the creep resistance of the material, but the decrease in minimum creep rate with increased amounts of prestrain indicates that a dispersion hardening effect still occurs.

One may contend that in spite of the higher density of cracks away from the fracture surface in the higher creep rate specimens, there is only one line that can be fit to all the points and not two distinct

.5 mm

Fig. 12. Photomicrograph of a specimen with a creep rate comparable to the average minimum creep rate at 0.6% prestrain.
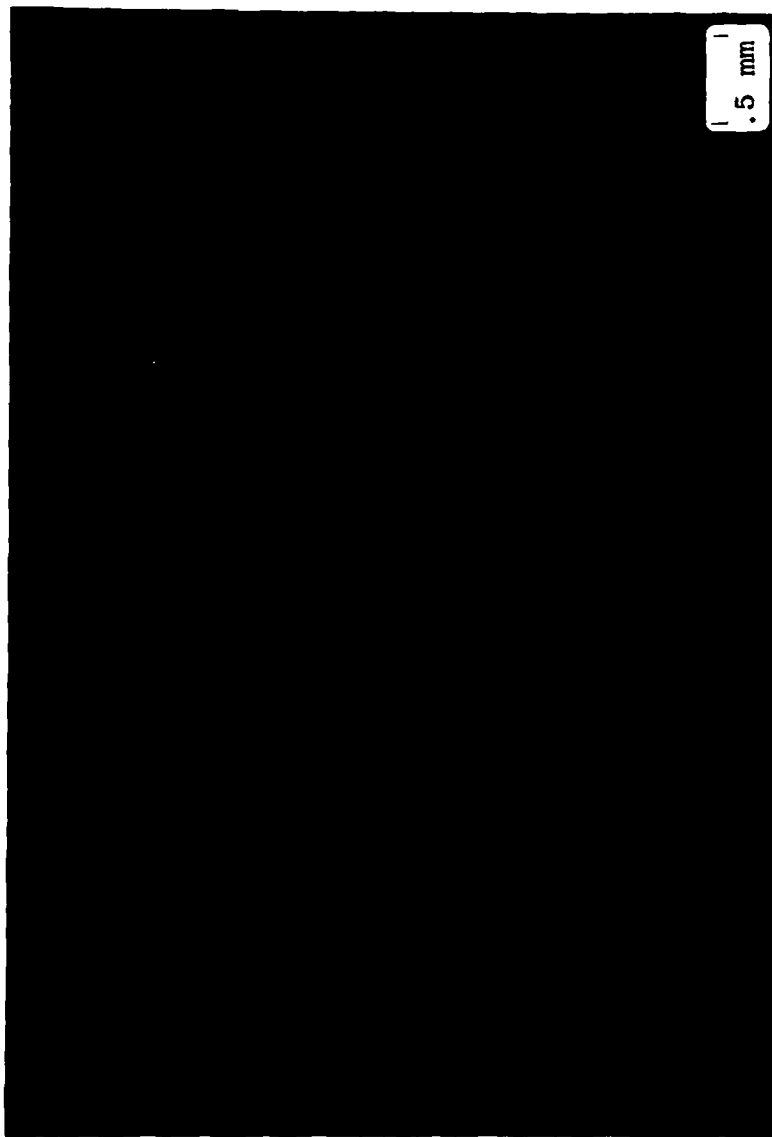
.5 mm

Fig. 13. Photomicrograph of a specimen with a creep rate comparable to the average minimum creep rate at 0.6% prestrain.
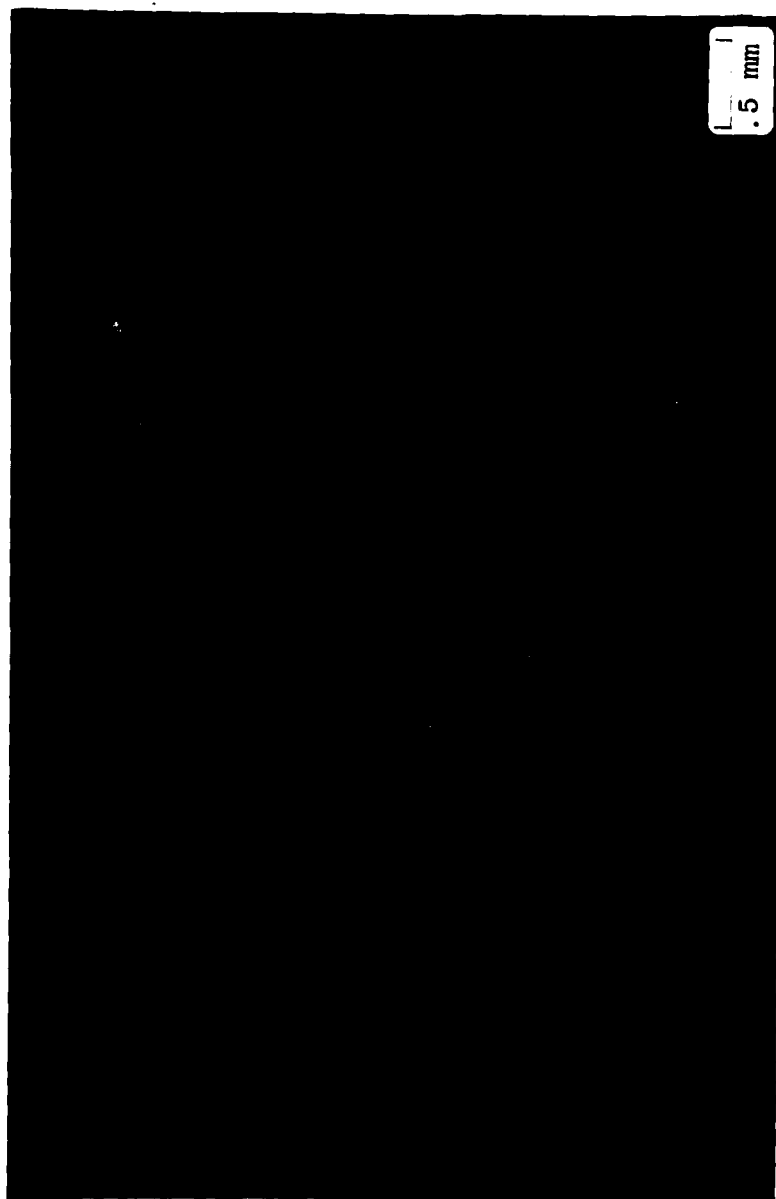
.5 mm

Fig. 14. Photomicrograph of a specimen with a creep rate nearly twice that of the average minimum creep rate at 0.6% prestrain.

lines as was assumed in this report. If one fits a line to all the points
by a least-squares linear regression, the correlation coefficient, which
is a measure of the "degree of fit" of the given points to the least-square
line, is calculated to be 53.7%. On the other hand, the correlation coef-
ficients of lines fit separately to the higher creep rate points and the
normal creep rate points are 93.2% and 91.5% respectively.

If one line is fit to the data, one finds that the minimum creep rate
still decreases with increasing amounts of prestrain (Figure 16). However,
a plot of the average rupture life versus amount of prestrain, using all
the points, shows a slight increase in the rupture life up to 0.9% prestrain
and then a decrease (Figure 17). A short rupture life can be attributed to
premature failure caused by defects in a specimen, but a long rupture life
has to be accounted for in some way. Figure 17 shows that the long rupture
lives at the 0.6% prestrained condition are longer than those at the 0.9%
condition, and the curve does not reflect this observation. In other words,
a single curve ignores the long rupture lives which must be accounted for.
If separate curves are plotted for the higher creep rate specimens and the
normal creep rate specimens, the curve for the normal specimens reflects
the longer rupture lives at 0.6% prestrain.

The apparent increase in the rupture lives of the specimens with the
higher creep rates (Figure 5) with increasing amounts of prestrain may be
due to stress relaxation around the defects. The stresses around defects
may be relieved by local deformation caused by the prestraining process.
At 0.3% prestrain, the deformation may not be sufficient to relieve the
stresses and, therefore, cracking occurs in the vicinity of the defects
causing a shortened rupture life. As the amount of prestrain increases,
more of the stresses around the defects are relieved by deformation and
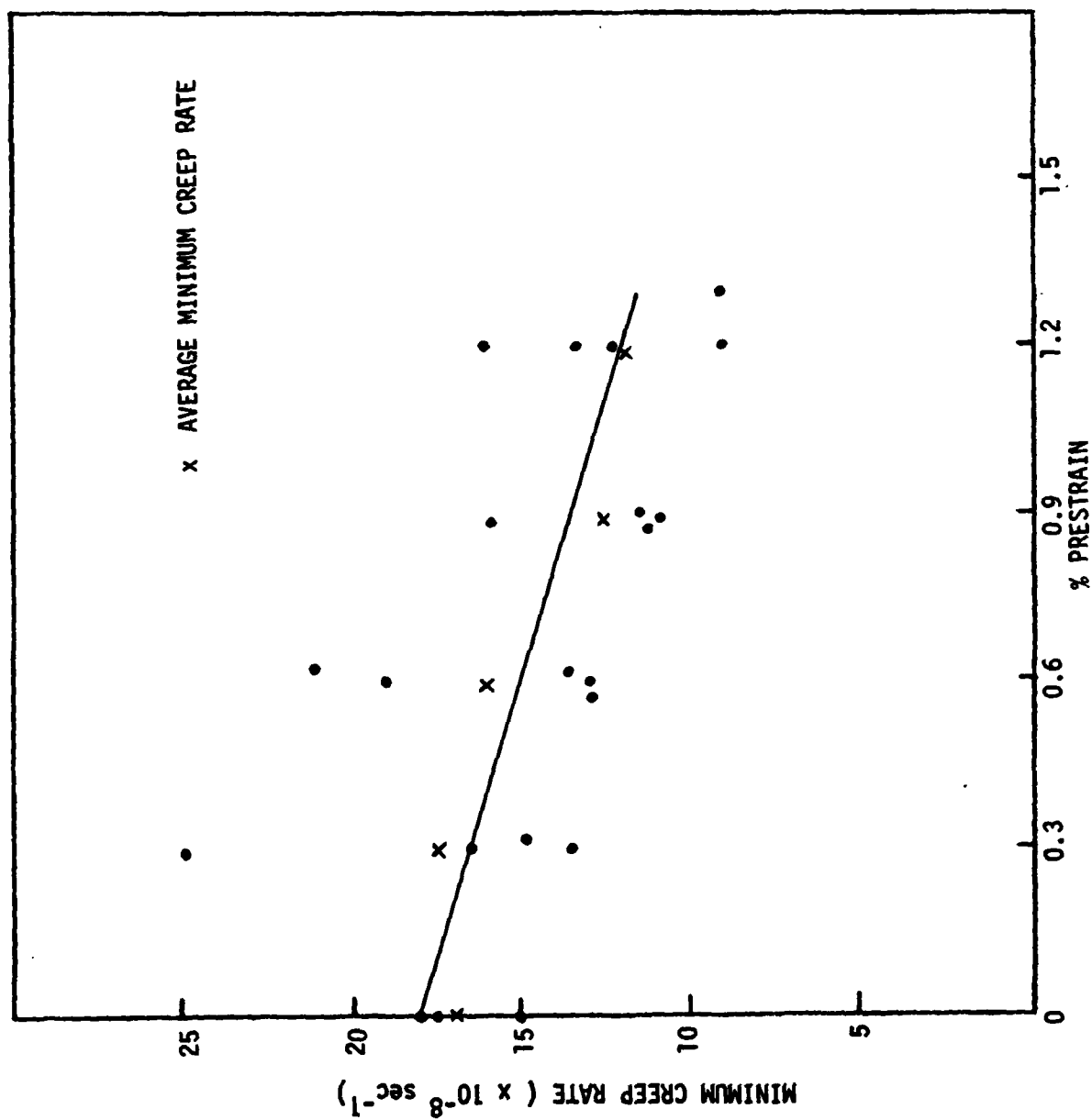the rupture life increases.

Fig. 16. Graph of minimum creep rate versus amount of prestrain using all the data points.
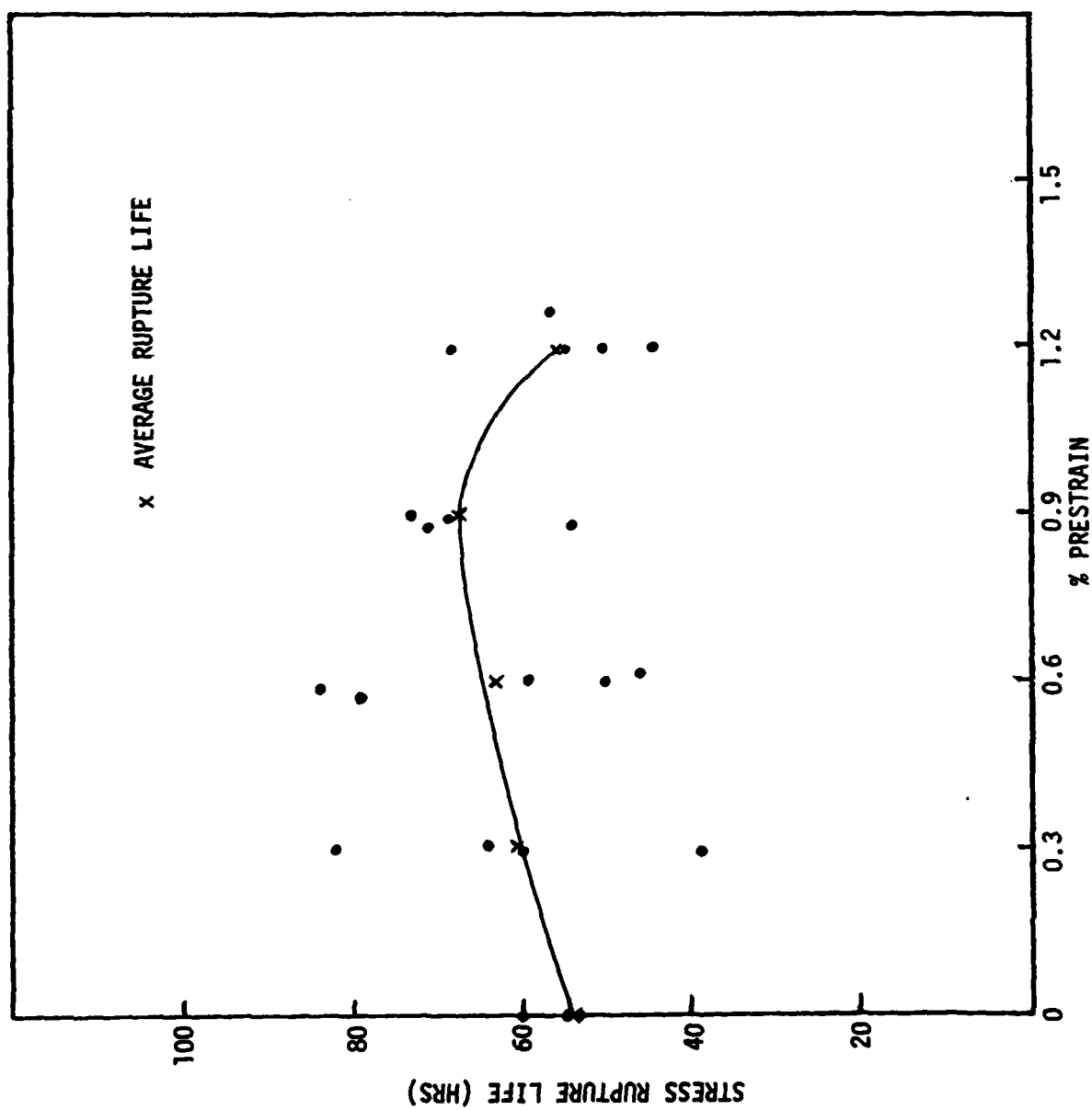
Fig. 17. Graph of stress rupture life versus amount of prestrain using all the data points.

It is interesting to note that the lines for both the higher strain rate points and the "normal" strain rate points seem to converge at some value greater than the 1.2% prestrain value (Figure 4). In order to converge, the decrease in minimum creep rates for the higher strain rate specimens must be greater than the decrease in the normal specimens. The larger decrease in the minimum creep rates for the higher creep rate specimens with increasing amounts of prestrain may be attributed to a combination of the dispersion hardening and stress relaxation effects. As the amount of prestrain increases, the stresses which cause cracking around defects are relaxed and the specimens are less susceptible to premature cracking and, in essence, become more creep resistant. This effect combined with the dispersion hardening effect caused by the predeformation process may account for the larger decrease in the minimum creep rates of the higher creep rate specimens, causing the convergence of the curves.

As alluded to in the introduction, this study was undertaken in order to determine if the creep and stress rupture properties of MA 754 change due to deformation caused by high stresses around a notch tip, and if the properties are altered, can a notch strengthening effect be explained in terms of the change in properties. The creep rate and stress rupture life of MA 754 after predeformation are definitely affected and the changes can contribute to a notch strengthening effect. However, a geometric effect still may exist, and strengthening may be due to a combination of both geometric and dispersion hardening effects.

V. CONCLUSIONS

Predeformation by small amounts of tensile creep has a definite effect on the creep and stress rupture properties of MA 754. This predeformation causes dislocation emission at particle-matrix interfaces, and the dislocations are pinned by the dispersion of oxide particles, thereby increasing the creep resistance of the material. The average minimum creep rate decreases with increasing amounts of prestrain due to the dispersion hardening effect.

The average stress rupture life increases up to 0.6% prestrain, but then decreases due to an early onset of the tertiary creep stage caused by accumulated strain damage. There is evidence of a strain controlled failure criterion.

A change in the creep and stress rupture properties of the material due to high stresses around a notch tip can account for the notch strengthening observation in MA 754, but it is not known whether the effect is solely responsible for the strengthening. A geometric effect may still exist, and the notch strengthening may be due to a combination of both geometric and dispersion hardening effects.

REFERENCES

1. F. Nami, Master's Thesis, Columbia University, New York (1979)

2. D.R. Hayhurst and J.T. Henderson, Creep Stress Redistribution in Notched Bars, Int. J. Mech. Sci., Vol. 19, PP. 133-146.

3. R.L. Cairns, L.R. Curwick, and J.S. Benjamin, Met. Trans., 1975, Vol. 6A, p. 179.

4. J.S. Benjamin and M.J. Bomford, Met. Trans., 1974, Vol. 5, p. 615.

5. J.S. Benjamin, T.E. Volin, and J.H. Weber, High Temperatures-- High Pressures, 1974, Vol. 6, p. 443.

6. Y. Beers, Introduction to the Theory of Error (Addison-Wesley, New York, 1957).

7. P.B. Hirsch, A. Howie, R.B. Nicholson, D.W. Pashley, and M.J. Whelan, Electron Microscopy of Thin Crystals, 1965, pp. 422-423.

8. M.F. Ashby, S.H. Gelles, and L.E. Tanner, The Stress at which Dis- locations are Generated at a Particle-Matrix Interface, Phil. Mag., 1969, No. 160, pp. 757-772.

9. T.E. Howson, J.E. Stulga, and J.K. Tien, Creep and Stress Rupture of Oxide Dispersion Strengthened Mechanically Alloyed MA 754, Columbia University paper submitted for publication.

10. T.E. Howson, Eng. Sc. D. Thesis, Columbia University, New York (1979).